

periodic variability, attributed to the T-dwarf Luhman 16B, and combined with a fast evolution of the observed patterns.

The next section presents our TRAPPIST data and their reduction. Our analysis of the resulting photometric time-series is described in Sec. 3. Finally, we discuss briefly our results in Sec. 4.

2. Data description

We monitored WISE 1049-5319 for twelve nights between 2013 March 14 and 26 with the robotic 60cm telescope TRAPPIST (*TR*ansiting *P*lanets and *P*lanetes/*I*mals *S*mall *T*elescope; Gillon et al. 2011, Jehin et al. 2011) located at ESO La Silla Observatory in the Atacama Desert, Chile. TRAPPIST is equipped with a thermoelectrically-cooled $2K \times 2K$ CCD having a pixel scale of $0.65''$ that translates into a $22' \times 22'$ field of view. The observations were obtained with an exposure time of 115s, with the telescope focused and through a special ‘ $I+z$ ’ filter having a transmittance $>90\%$ from 750 nm to beyond 1100 nm¹. Considering the transmission curve of this $I+z$ filter, the spectral response curve of the CCD detector, and the spectral type of the target, we derive an effective wavelength $\sim 910\text{nm}$ for the observations. The positions of the stars on the chip were maintained to within a few pixels over the course of each run, thanks to a ‘software guiding’ system deriving regularly an astrometric solution for the most recently acquired image and sending pointing corrections to the mount if needed.

After a standard pre-reduction (bias, dark, flatfield correction), the stellar fluxes for each run were extracted from the images using the IRAF/DAOPHOT² aperture photometry software (Stetson, 1987). The same photometric aperture of 8 pixels ($\sim 5.1''$) was used for all nights. After a careful selection of stable reference stars of similar brightness, differential photometry was then obtained. Finally, the light curves were normalized. The twelve resulting light curves are shown in Fig. 1. To assess the night-to-night variability of the target, we also extracted a global differential light curve that is shown in Fig. 2.

The typical full-width at half maximum of TRAPPIST point-spread function (PSF) is ~ 3 pixels = $\sim 2''$. At this resolution, the two components of the $1.5''$ binary are only partially resolved, and our photometry extracted with an aperture of $\sim 5.1''$ radius shows thus the evolution of the sum of the fluxes of both components.

3. Data analysis

While being relatively stable on longer timescales (Fig. 2), Luhman 16 shows a clear variability on a nightly timescale (Fig. 1). Furthermore, the observed patterns evolve strongly from one night to the other. A Lomb-Scargle periodogram (Lomb 1976; Scargle 1982) applied to our photometry shows a strong power excess around $\sim 0.2\text{d}$, matching well the typical separation between similar features in the light curves.

We performed a global analysis of our twelve light curves, adapting for that purpose the Markov Chain Monte Carlo (MCMC) code described in Gillon et al. (2012, hereafter G12). In a first step, we assumed that the observed variability was originating from only one of the two BDs. Our basic model for the ro-

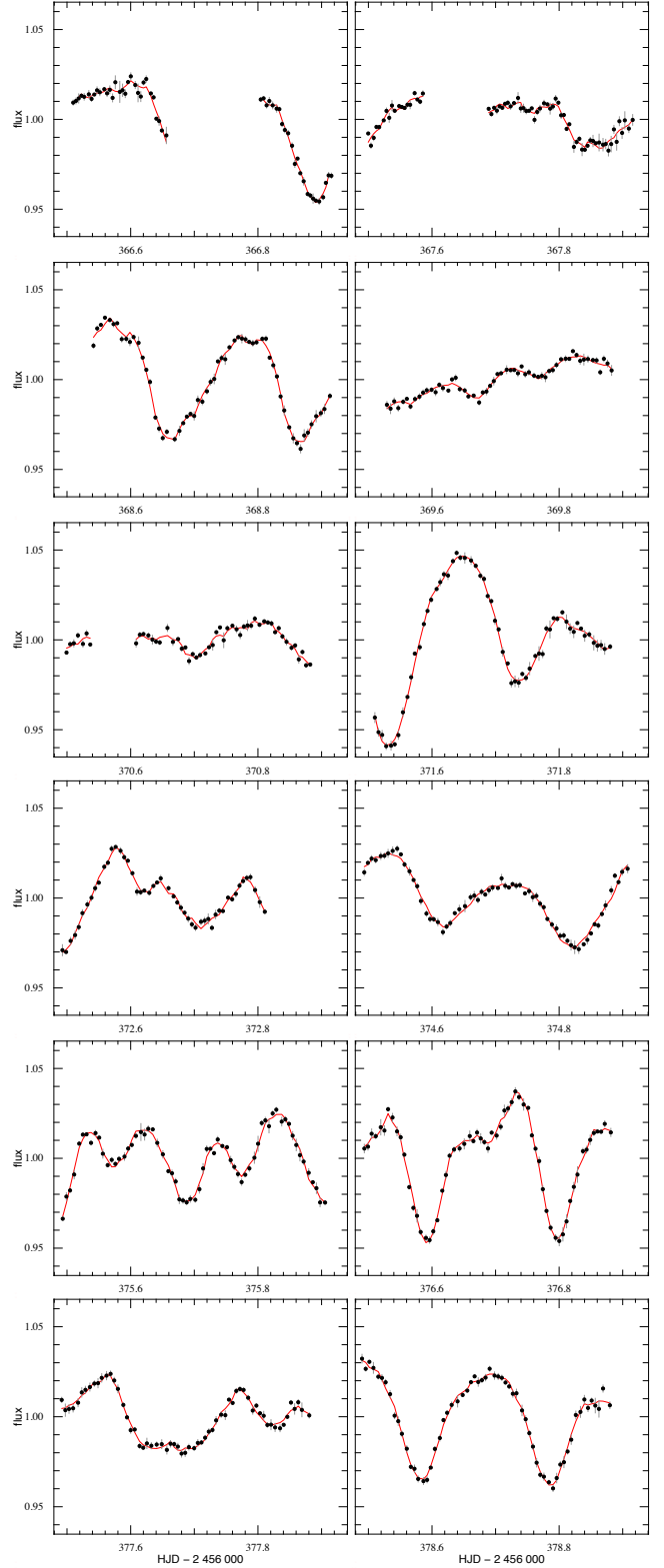


Fig. 1. Normalized TRAPPIST light curves for Luhman 16 binned per 10 min intervals. For each light curve, the best-fit global model (see Sec. 3) is over-imposed in red. Gaps for night #1 and #5 correspond to cloudy conditions. The gap for night #2 corresponds to the observation of another target.

tational modulation was based on a division of the brown dwarf into 10 longitudinal slices. For each of them, the surface flux was assumed to be constant during each night, the measured flux be-

¹ <http://www.astrodon.com/products/filters/near-infrared/>

² IRAF is distributed by the National Optical Astronomy Observatory, which is operated by the Association of Universities for Research in Astronomy, Inc., under cooperative agreement with the National Science Foundation.

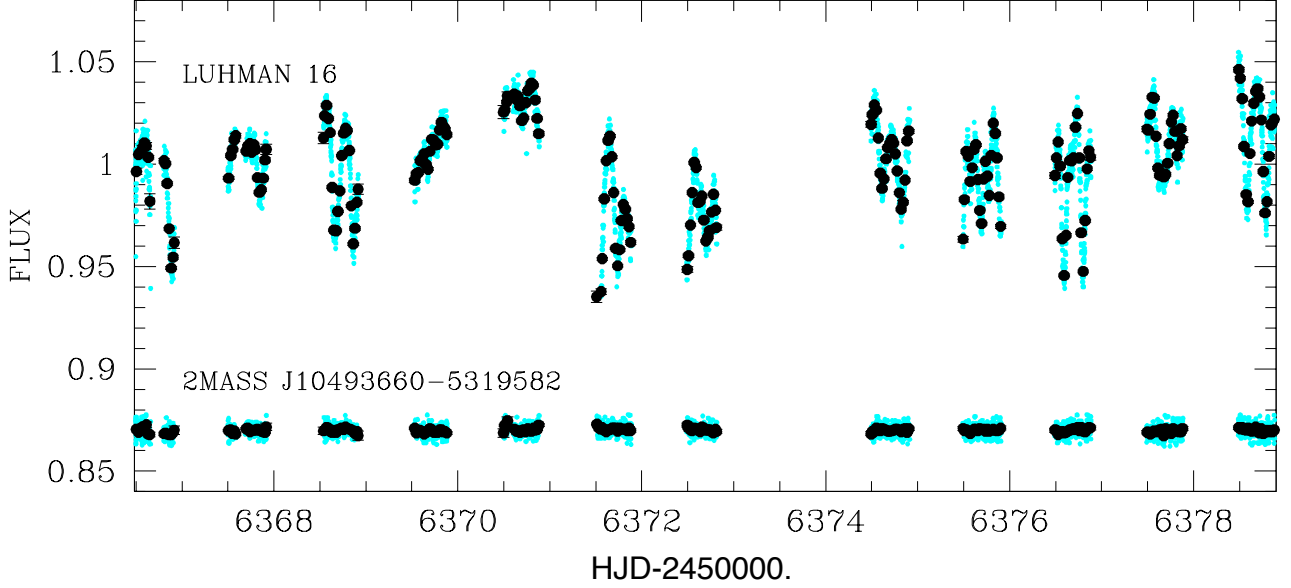


Fig. 2. Globally normalized TRAPPIST differential photometry for Luhman 16 (*top*) and for one of the comparison stars used in the reduction (*bottom*, shifted along the *y*-axis for the sake of clarity), unbinned (*cyan*) and binned per interval of 30 min (*black*). The standard deviation of the binned light curves are 2.2% and 0.1% for Luhman 16 and the comparison star, respectively.

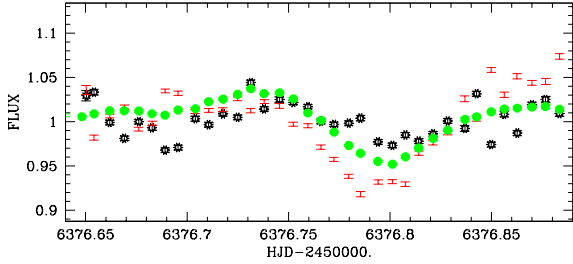


Fig. 3. Differential photometry for the second part of night #10, binned per 10 min intervals, obtained with an aperture encompassing both components of the binary (*filled green circles*), and with apertures encompassing only the PSF center of Luhman 16A (*black empty symbols*) and Luhman 16B (*red vertical bars*). The amplitude of the variations is amplified on Luhman 16B, indicating that they originate from this T-dwarf.

ing modeled by a semi-sinusoidal function falling to zero when the slice disappears from view. To this rotational model, we added a baseline model accounting for (i) the flip of the equatorial mount of the telescope at the meridian, putting the stellar images on different pixels and thus possibly creating small offsets in the differential photometry, (ii) a 2^{nd} -order airmass polynomial aiming to model the differential extinction curvature due to the much redder color of the target compared to the comparison stars, and (iii) a 4^{th} -order time polynomial representing the low-frequency variability of the system, including the evolution of the patterns from one rotation to the other. In this global model, the only two perturbed parameters in the MCMC were the rotation period and an arbitrary phase, the solution for the remaining parameters being obtained by linear regression at each step of the Markov chains (see G12 for details). Two MCMC chains of 100,000 steps were performed to probe efficiently the posterior distribution of the rotational period.

Our MCMC analysis gives $P_{rot} = 4.87 \pm 0.01h$, producing an excellent fit between the model and the data (see Fig. 1). While a periodogram of the residuals reveals no additional period, we performed an additional analysis by adding a second rotational model to the MCMC. This analysis also failed to identify a second period. The Bayesian Information Criterion (Schwarz 1978) significantly increased by +360, indicating that a model including a single rotation period is a more likely representation of the data. We thus conclude that only one of the two BDs dominates the photometric variability since a same rotational period for both BDs is unlikely.

A new photometric reduction of a fraction of our images using the IRAF/DAOPHOT ALLSTAR PSF-fitting software (Stetson 1987) revealed that the B component is -0.1 ± 0.1 mag brighter than the A component

We then attempted to determine the origin of the signal. We extracted the fluxes of both components by aperture photometry, fixing the aperture centers on the known positions of the two BDs. The aperture sizes were chosen to encompass only one PSF center. Using only data showing both a large signal and having the smallest and most stable PSF widths, we find that a larger amplitude is visible on the T-dwarf, while no significant signal is obtained for the L-dwarf. This is illustrated for a fraction of night #10 in Fig. 3. From these results, we conclude that the detected quasi-periodic variability originates from the T-dwarf Luhman 16B.

4. Discussion

From their new spectroscopy and from the relationship of Stephens et al. (2009), K13 attribute to Luhman 16A and B components effective temperatures of $1350 \pm 120K$ and $1220 \pm 110K$, respectively. Such very low temperatures make atmospheric condensates the most likely source of the observed rotational variability (see discussion by Radigan et al. 2012 for the T1.5 BD 2M2139). The most surprising feature of the patterns reported here is their fast evolution from night to night. To our knowledge,

this is the first time that such rapid evolution is reported for the cloud coverage of an L/T transition BD, making Luhman 16B an actual ‘Rosetta Stone’ for the study of BDs atmospheres. Future multi-band and high-cadence spectroscopic time-series will be able to observe while clouds condensate and are then dispersed, giving unprecedented access into the physico-chemical processes acting in such atmospheres.

Considering our measured $\Delta\text{mag} = 0.1 \pm 0.1$ between both BDs, the variability amplitudes visible in Fig. 1 are thus diluted by a factor ~ 2 by the blend of both PSFs in the TRAPPIST images. The actual maximal peak-to-peak variability amplitude of Luhman 16B should thus be $>20\%$. Similar amplitudes were observed around $1\mu\text{m}$ for at least another early T-dwarf, the T1.5-type BD 2M2139 (Radigan et al. 2012). For the L-dwarf Luhman 16A, we do not detect any variability, but our sensitivity is limited by the partial resolution of both components in our images. High-cadence photometry with a better spatial resolution will be needed to thoroughly assess its photometric variability.

Binary stars have been used from the dawn of modern astronomy as a means to control some variables, while leaving others free. In our case both BDs probably formed together out of the same fragment; they should have their age and composition on a par. What differentiates them is their mass. This affects their respective effective temperatures and densities. Although only 100 K apart, that one shows clouds breaking while the other does not is an indication of how sharp the boundary from a stable to an unstable atmosphere is, and of how closely tuned it must be to effective temperature and scale height.

Field BDs are very interesting targets for exoplanets transit searches (Blake et al. 2008; Bolmont et al. 2011; Belu et al. 2013), as their small sizes make possible the detection of terrestrial planets with photometric precisions at the mmag level similar to the ones reported here for Luhman 16. A careful visual inspection of the residuals light curves and a search for periodic box-like patterns with the BLS algorithm (Kovacs et al. 2002) failed to detect any transit-like signal. Despite the blend of both BDs, our sensitivity is good enough to partially probe the terrestrial regime. Fig. 4 (top panel) shows the residuals of our global modeling compared to the expected transit depths for a $2R_{\oplus}$ radius planet, for both BDs, assuming for each of them a $0.1R_{\odot}$ radius. The corresponding transit is firmly discarded by our data. For orbital periods smaller than the mean duration of our runs ($\sim 9.5\text{h}$), our detection threshold goes down to Earth-size planets, as can be seen in Fig. 4 (bottom panel). This shows that intensive campaigns like the one described here targeting the most nearby field BDs with small to medium-sized ground-based telescopes or, better, with an infrared space facility like *Spitzer* (Triaud et al. in prep.) could efficiently assess the frequency of close-in terrestrial planets around BDs, possibly detecting Earth-sized planets amenable for atmospheric characterization with, e.g., JWST (Belu et al. 2013).

Acknowledgements. The authors thank Mark S. Marley for his valuable suggestion. TRAPPIST is a project funded by the Belgian Fund for Scientific Research (Fonds National de la Recherche Scientifique, F.R.S-FNRS) under grant FRFC 2.5.594.09.F, with the participation of the Swiss National Science Foundation (SNF). M. Gillon and E. Jehin are FNRS Research Associates. A.H.M.J. Triaud is Swiss National Science Foundation fellow under the grant PBGE2-145594. C. Opitom and L. Delrez thank the Belgian FNRS for funding their PhD theses.

References

Ackerman, A. S., & Marley, M. S. 2001, *ApJ*, 556, 872
 Artigau, E., Bouchard, S., Doyon, R., Lafrenière, D. 2009, *ApJ*, 701, 1534
 Apai, D., Radigan, J., Buenzli, E., et al., 2013, *ApJ* (in press), arXiv:1303.4151

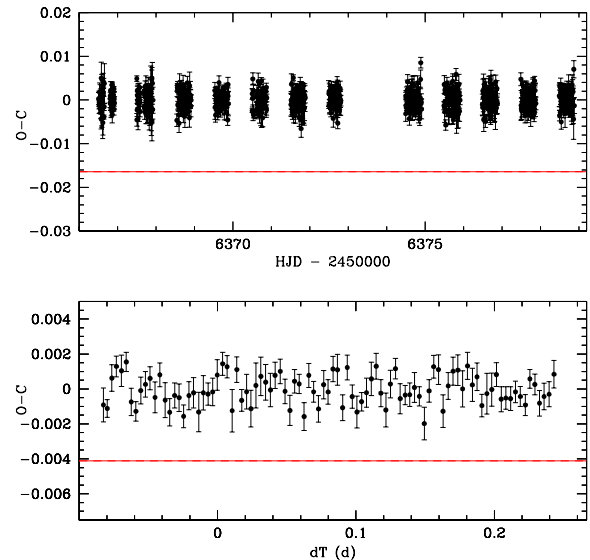


Fig. 4. Residuals of our global modeling, unfolded and binned per 10 min intervals (*top*), folded with $P = 8\text{h}$ and binned per 5 min intervals (*bottom*). For the unfolded residuals is shown as a red horizontal line the expected transit depth for a $2R_{\oplus}$ planet orbiting one of the two BD, assuming a $0.1R_{\odot}$ radius and the same brightness for both BDs. The same is done for the folded residuals, but assuming a $1R_{\oplus}$ planet.

- Belu, A. R., Selsis, F., Raymond, S. N., et al. 2013, *ApJ* (in press), arXiv:1301.4453
 Bolmont, E., Raymond, S. N., Leconte, J. 2011, *A&A*, 535, 94
 Blake, C. H., Bloom, J. S., Latham, D. W., et al. 2008, *PASP*, 120, 860
 Burgasser, A. J., Sheppard, S. S., & Luhman, K. L. 2013, *ApJ* (submitted), arXiv:1303.7283
 Clarke, F. J., Hodgkin, S. T., Oppenheimer, B. R., et al. 2008, *MNRAS*, 386, 2009
 Gillon, M., Jehin, E., Magain, P., et al. 2011, *Detection and Dynamics of Transiting Exoplanets*, Proceedings of OHP Colloquium (23-27 August 2010), eds. F. Bouchy, R. F. Diaz & C. Moutou, Platypus Press, 06002
 Gillon M., Triaud A. H. M. J., Fortney J. J., et al. 2012, *A&A*, 542, 4
 Herbst, W., Eisloffel, J., Mundt, R., & Scholz, A. 2007, *Protostars and Planets V*, B. Reipurth, D. Jewitt, and K. Keil (eds.), University of Arizona Press, Tucson, 951, 297
 Khandrika, H., Burgasser, A. J., Melis, C., et al. 2013, *AJ*, 145, 71
 Kovacs, G., Zucker, S., & Mazeh, T. 2002, *A&A*, 391, 369
 Jehin, E., Gillon, M., Queloz, D., et al. 2011, *The Messenger*, 145, 2
 Kirkpatrick, J. D. 2005, *ARA&A*, 43, 195
 Kniazev, A. Y., Vaisanen, P., Muzic, K., et al., 2013, *ApJL* (submitted), arXiv:1303.7171
 Lomb, N. R., 1976, *Ap&SS*, 39, 447
 Luhman, K. L. 2013, *ApJL* (in press), arXiv:1303.2401
 Mamajek, E. E. 2013, arXiv:1303.5345
 Mayor, M., & Queloz D. 1995, *Nature*, 378, 355
 Rebolo, R., Zapatero Osorio, M. R., & Martín, E. L. 1995, *Nature*, 377, 129
 Radigan, J., Jayawardhana, R., Lafrenière, D., et al. 2012, *ApJ*, 750, 105
 Saumon, D., & Marley, M. S. 2008, *ApJ*, 689, 1327
 Scargle, J. D., 1982, *ApJ*, 263, 835
 Schwarz, G. E. 1978, *Annals of Statistics*, 6, 461
 Seager, S., & Deming, D. 2010, *Exoplanets Atmospheres*, ARAA, 48, 631
 Showman, A. P., & Kaspi, Y. 2012, *ApJ* (submitted), arXiv:1210.7573
 Stephens, D. C., Leggett, S. K., Cushing, M. C., et al. 2009, *ApJ*, 702, 154
 Stetson, P. B. 1987, *PASP*, 99, 111
 Vrba, F. J., Henden, A. A., Luginbuhl, C. B., et al. 2004, *AJ*, 127, 2948